

Your Room is not Private: Gradient Inversion Attack for Deep Q-Learning

Miao Li

Carnegie Mellon University
limiao@andrew.cmu.edu

Wenhao Ding

Carnegie Mellon University
wenhaod@andrew.cmu.edu

Ding Zhao

Carnegie Mellon University
dingzhao@cmu.edu

Abstract: The prominence of embodied Artificial Intelligence (AI), which empowers robots to navigate, perceive, and engage within virtual environments, has attracted significant attention, owing to the remarkable advancements in computer vision and large language models. Privacy emerges as a pivotal concern within the realm of embodied AI, as the robot access substantial personal information. However, the issue of privacy leakage in embodied AI tasks, particularly in relation to decision-making algorithms, has not received adequate consideration in research. This paper aims to address this gap by proposing an attack on the Deep Q-Learning algorithm, utilizing gradient inversion to reconstruct states, actions, and Q-values. The choice of using gradients for the attack is motivated by the fact that commonly employed federated learning techniques solely utilize gradients computed based on private user data to optimize models, without storing or transmitting the data to public servers. Nevertheless, these gradients contain sufficient information to potentially expose private data. To validate our approach, we conduct experiments on the AI2THOR simulator and evaluate our algorithm on active perception, a prevalent task in embodied AI. The experimental results convincingly demonstrate the effectiveness of our method in successfully recovering all information from the data across all 120 room layouts.

Keywords: Privacy, Reinforcement Learning, Gradient Inversion

1 Introduction

The advent of recent large foundation models has brought about remarkable achievements in human-like dialog generation [1] and controllable image generation [2]. These accomplishments highlight the promising potential of leveraging artificial intelligence (AI) to enhance human experiences. The next significant milestone in the advancement of general AI revolves around the exploration of embodied systems, such as household robots, that possess the ability to navigate, perceive, engage, and successfully tackle tasks within the physical world.

The process of collecting embodied datasets presents more privacy concerns in comparison to language and vision tasks, as the robot operates within real-world environments, executing policies and gathering observational signals. These environments often contain personal information [3, 4], which introduces challenges during data collection and model training. To address the need for preserving sensitive information, the *Federated Learning* framework [5] is introduced. This framework allows for the local storage of private data on individual machines, with only the gradients, calculated based on the private information within the environment [6, 7, 8, 9], being transmitted to the central server. These gradients, originating from multiple private servers, are then aggregated and utilized to update the policy model on the central server. The updated model is subsequently sent back to the private servers for the next optimization iteration. As a result, the model and gradients are accessible publicly, while the data remains accessible only to private servers.

However, relying solely on the transmission of gradients still leaves room for vulnerability to gradient inversion techniques [10, 11, 12, 13], a type of method that can recover input images and labels

from the corresponding gradients in classification tasks. The gradient inversion algorithms either search for realistic synthetic images in latent spaces using generative networks [14] or directly optimize a synthetic image in the image domain, initialized by heuristic methods. The accuracy of recovery is optimized by a loss function that compares the real gradient sent by the private server with the gradient produced using the synthetic data. Concurrently, the visual quality of the recovered image is ensured through loss functions based on prior knowledge, such as the smoothness of natural images [10, 15, 11, 12]. These techniques can recover high-resolution images with recognizable patterns using gradients from mini-batches with small batch sizes [11, 16]. Although not all recovered images are necessarily recognizable, these studies highlight the privacy risks associated with federated learning.

Motivated by the existing literature on gradient inversion in classification tasks, our research aims to address the privacy leakage issue in decision-making within the context of embodied AI, an area that has received limited attention thus far. Figure 1 provides an illustrative example of this problem, demonstrating how an attacker can successfully reconstruct RGB and depth images of a room solely from the gradient.

Unlike in classification tasks where the input typically consists of a single RGB image, applying gradient inversion techniques to decision-making poses unique challenges due to the multi-modal nature of the input information including image state, vector state, action, and reward. Our objective is to recover all these inputs exclusively from the gradients shared by the decision-making algorithm. The most relevant work to this topic is [17], which recovers the location map from the model parameter of Deep Q Network (DQN) [18]. However, this approach is limited in that it supports only one map for one model, and accessing the parameters of trained models may not be feasible in typical scenarios.

In this work, we introduce a novel approach called *Deep Q-learning Gradient Inversion (QGI)* to address the task of recovering multi-modal inputs from the Q-learning reinforcement learning (RL) algorithm. Specifically, we initialize the reconstructed state with Gaussian noises and optimize it with cosine similarity between the gradients of the real and reconstructed state. An additional prior term is used to penalize noisy image patterns. Unlike in classification tasks where the input is only RGB images, gradient inversion in reinforcement learning is challenging due to the multi-modal input information. We follow the white-box assumption [19] and honest-but-curious assumption [11] of the potential adversary, which does not modify the model or the optimization process. We evaluate QGI in the AI2THOR [20] simulator on the active perception task [21, 22, 23], a popular in embodied AI to navigate agents to obtain higher detection accuracy of the given object. Our main contributions are summarized below:

- As far as we know, QGI is the first framework to investigate the information leaking problem by recovering data in reinforcement learning from the gradient.
- QGI provides a novel pipeline to recover multi-modal information of states, actions, and Q values, which outperforms the joint optimization method proposed by previous works.
- We evaluate our method in a realistic simulation of the active perception task and show that our QGI can successfully recover all information from the data across all 120 room layouts.

2 Preliminary

Gradient Inversion. Gradient inversion aims to recover the training data from the gradient of the model, which can be employed by the potential adversary when the training data is invisible but the gradient is shared, for example, in federated learning. Given the input of the network x , the supervision signal u (e.g., label in classification), the model F with parameters w , the output

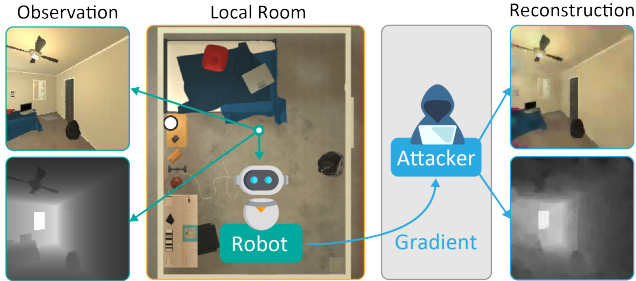


Figure 1: Our method (Attacker) can reconstruct the images of your untidy room and window orientation from the gradient of the model in the robot.

$y = F(x; w)$, and the objective function J , then the gradient g is

$$g = \nabla_w J(F(x; w), u) = \frac{\partial J(y, u)}{\partial y} \frac{\partial F(x; w)}{\partial w}. \quad (1)$$

The gradient carries the information of x in the calculation $\frac{\partial F(x; w)}{\partial w}$ and the information of u in the $\frac{\partial J(y, u)}{\partial y}$, which can be utilized by an honest-but-curious [11, 17] adversary to reconstruct the (x, u) . The objective of gradient inversion is to generate (x^{rec}, u^{rec}) that produces gradient g^{rec} , which is sufficiently close to the true gradient g . Assuming the adversary has white-box access to the model F and the objective J , then the reconstructed gradient is $g^{rec} = \nabla_w J(F(x^{rec}; w), u^{rec})$. The adversary minimizes the loss function $L(g^{rec}, g) = \arg \min_{\tilde{x}, \tilde{u}} L(\tilde{g}(\tilde{x}, \tilde{u}), g(x, u))$.

Markov Decision Process (MDP) and DQN. We consider Markov Decision Process (MDP) as the mathematical framework to model decision-making problems in reinforcement learning. MDP is consist of state space $s \in \mathcal{S}$, action space $a \in \mathcal{A}$, reward function $r \in \mathcal{R}$, and a transition model $p \in \mathcal{P}$. The future discounted return at timestep t is $R_t = \sum_{t'=t}^T \gamma^{t'-t} r_{t'}$, where γ is the discount factor and T is the maximal step. In this paper, we investigate the gradient inversion in the DQN algorithm [18], which estimate the optimal action-state value function (Q-value) $Q^*(s, a) = \max_{\pi} \mathbb{E}[R_t | s_t = s, a_t = a, \pi]$, where π is a policy mapping sequences to actions. Empirically, this $Q^*(s, a)$ is parameterized with neural networks and the objective is minimizing the difference between the predicted Q-value $\hat{Q}(s, a)$ of the selected action a and the target Q-value $Q(s, a)$ with transitions (s_t, a_t, s_{t+1}, r_t) from the replay buffer.

Active Perception Task. Active Perception [21, 22, 23] is a prevalent embodied AI task to enable robots to capture data in a better position to increase the confidence and accuracy of detection. Since it requires private information about the user room, we select it as the example task to apply the gradient inversion attack. In this task, the state contains depth image s_d , RGB image s_i , and coordinate s_c that indicates the position of the target object in the images. The action space is discrete with seven movement options. Similar to [21], the reward is defined by the confidence score obtained from an object detection model. The policy network predicts Q-values $\hat{Q}(s, a)$ for all possible actions given the input $s = \{s_d, s_i, s_c\}$. The images are first processed by convolution layers F_{conv} , and the coordinate vector is processed by linear layers F_{linear} . The detailed network structure can be found in Appendix A.

3 Deep Q-Learning with Gradient Inversion (QGI)

In this section, we introduce QGI, a method to reconstruct the state s , action a , Q-value $\hat{Q}(s, a)$, and target Q-value $Q(s, a)$ by gradient inversion, which increases the accuracy of reconstruction compared to naive joint optimization. Note that reward is not recoverable as it is generated on the environment side with no gradient available. Despite we focus on the single sample gradient, the inversion of the batched gradient can also benefit from the insight. We show the entire pipeline in Figure 2 and organize this section with the following steps. In **step 1**, we first identify the action with gradient analysis. In **step 2**, we reconstruct the vector state and image state in two stages, where stage 1 targets the input of all linear layers, including the coordinate vector s_c and stage 2 reconstructs the image states s_d and s_i . In **step 3**, Q-value $\hat{Q}^{rec}(s, a)$ is obtained by applying the reconstructed vectors, and the target Q-value Q^{rec} is estimated by reconstructing the error $\hat{Q}(s, a) - Q(s, a)$.

3.1 Action Reconstruction

Since the action space of DQN is discrete, a naive way to recover action is to enumerate all dimensions. Instead of the computation-heavy enumeration, we propose to directly identify the action from the gradient when only 1 or 2 data samples are used to compute the gradient. The Q-value $\hat{Q}(s, \cdot)$ is obtained from a linear layer with weights W_{last} and bias b_{last} . In addition, the objective $J(\hat{Q}(s, a), Q(s, a))$ only provides a supervision signal to the action a that is taken by the policy,

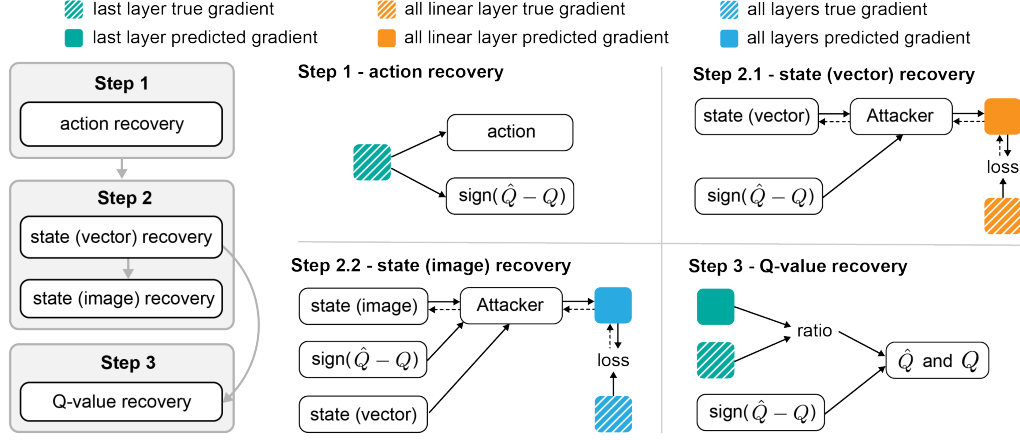


Figure 2: Pipeline of the proposed method. The left part shows the steps to reconstruct the multi-modal information, and the right part explains each step in detail.

thus we can obtain the action and the sign of error $\hat{Q} - Q$ from the gradient

$$\nabla_{b_{\text{last}}} = \frac{\partial J(\hat{Q}(s, a), Q(s, a))}{\partial \hat{Q}(s, a)} \underbrace{\frac{\partial \hat{Q}(s, a)}{\partial \hat{Q}(s)}}_{\text{one-hot vector}} \underbrace{\frac{\partial \hat{Q}(s)}{\partial b_{\text{last}}}}_1. \quad (2)$$

When $\frac{\partial J(\hat{Q}, Q)}{\partial \hat{Q}} \neq 0$, only the a -th element of b_{last} has a non-zero gradient, which allows us to reconstruct the action. When the batch size is larger than 2, actions may not be identified directly from the batched gradient, thus the reconstruction requires enumeration or optimization.

3.2 State Reconstruction

As shown in Figure 2, we separate the state reconstruction into 2 stages. We reconstruct the vector state in step 2.1 and then reconstruct the image state in step 2.2 based on the following reasons. First, the gradient inversion of linear layers is easier than convolution layers [11] because (1) linear layers contain more parameters than convolution layers; (2) the gradient of linear layers does not aggregate the dimensions of the input of the linear layer or the partial derivative of the output. The aggregation exacerbates the challenge as different samples may have the same aggregated results. Second, we observe that the vector input is usually combined with the visual information in the vector form, enabling the neglect of convolution layers during the vector state reconstruction. Third, as the error in the vector state reconstruction could result in a significant accuracy drop in image reconstruction, an accurately reconstructed vector state obtained before the image state reconstruction is beneficial. Therefore, given the multi-modal data in this task, we propose to first reconstruct the vector state that is not processed by any convolution layers and then reconstruct the image state that requires convolution with the vector state fixed.

Specifically, we initialize the coordinate and the image reconstruction with Gaussian noises and optimize them by minimizing the gradient matching loss $L(g^{\text{rec}}, g)$,

$$L(g^{\text{rec}}, g) = 1 - \frac{\langle g^{\text{rec}}, g \rangle}{\|g^{\text{rec}}\|_2 \|g\|_2} \quad (3)$$

The total variation (TV) loss [24] is added to step 2.2 for image state reconstruction to penalize noisy patterns, leading to the total loss $L_{\text{img}} = L(g^{\text{rec}}, g) + \lambda(\text{TV}(s_i) + \text{TV}(s_d))$, where λ is a scalar weight. Since λ is critical to influencing the ratio of gradients of two terms in L_{img} , we use a rule to automatically calculate λ with

$$\lambda = \frac{\|\partial L(g^{\text{rec}}, g) / \partial s_i^{\text{rec}}\|}{\|\partial \text{TV}(s_i^{\text{rec}}) / \partial s_i^{\text{rec}}\|}, \quad \Delta s_i^{\text{rec}} = \frac{\partial L(g^{\text{rec}}, g)}{\partial s_i^{\text{rec}}} + \lambda \frac{\partial \text{TV}(s_i^{\text{rec}})}{\partial s_i^{\text{rec}}}. \quad (4)$$

The gradient in (4) is then used to update s_i^{rec} . For updating s_d^{rec} , we use the same rule to adjust λ .

3.3 Q-value Reconstruction

The reconstruction of Q-values is implemented in 3 stages, (1) reconstructing the sign of the error $\tilde{n} = \text{sign}(\hat{Q} - Q)$, (2) reconstructing the magnitude of error $\hat{Q} - Q$, (3) reconstructing \hat{Q} by feeding the state reconstruction and Q based on the reconstructed \hat{Q} and the reconstructed error. The sign \tilde{n} can be directly identified from the gradient of the last linear layer together with action identification, as shown in Figure 2. The magnitude of the error is obtained from the ratio $\|g\|/\|g^{rec}\|$. Since the objective to update the Q network is the mean square error (MSE), the gradient of all model parameters w is the first equation in (5), and the relationship between the error and the magnitude of the gradient is shown in the second equation in (5) with \tilde{Q} a constant to guess the target Q-value.

$$g = \frac{\partial J(\hat{Q}, Q)}{\partial \hat{Q}} \frac{\partial \hat{Q}}{\partial w} = 2(\hat{Q} - Q) \frac{\partial \hat{Q}}{\partial w}, \quad \left\| \frac{\hat{Q}(s, a) - Q(s, a)}{\hat{Q}^{rec}(s^{rec}, a^{rec}) - \tilde{Q}} \right\| \frac{\partial \hat{Q}/\partial w}{\partial \hat{Q}^{rec}/\partial w} = \frac{\|g\|}{\|g^{rec}\|}. \quad (5)$$

Once the g^{rec} is obtained in step 2.1 in Figure 2, we assume $\partial \hat{Q}/\partial w = \partial \hat{Q}^{rec}/\partial w$, and then get

$$\left\| \hat{Q}(s, a) - Q(s, a) \right\|^{rec} = \left\| \hat{Q}^{rec}(s^{rec}, a^{rec}) - \tilde{Q} \right\| \frac{\|g\|}{\|g^{rec}\|}, \quad (6)$$

where $\hat{Q}^{rec}(s^{rec}, a^{rec}) = F(s^{rec}, a^{rec}; w)$ is the reconstruction of $\hat{Q}(s, a)$. Then, the reconstruction of the target Q-value can be obtained below,

$$Q^{rec}(s, a) \leftarrow \hat{Q}^{rec}(s^{rec}, a^{rec}) - \tilde{n} \left\| \hat{Q}(s, a) - Q(s, a) \right\|^{rec}. \quad (7)$$

4 Experiment

Experimental setup. We conducted evaluations of our method on an active perception task using the AI2THOR simulator [20]. In the primary setting (S1), private observations were collected using an RGB camera and a depth camera, each providing an image with a resolution of 150×150 . Additionally, we explored the performance in a setting where only a depth camera was available (S2), aiming to examine the privacy risks associated with widely used depth images in robotic tasks. The target object’s 4-dimensional coordinate was specified by the upstream task within the range of $[-1, 1]$. Gradients were calculated for individual data samples fed into an initialized network. We also study gradient inversion for a trained network in setting S2, please refer to Appendix B. The reconstruction process for both step 2.1 and step 2.2 involved 2×10^4 iterations. Quantitative evaluation was performed using 240 pre-collected samples. For more detailed information about the hyperparameters employed, please refer to Appendix C.

Metric. To assess the quality and accuracy of the recovered state, action, Q-value, and target Q-value, we have selected several metrics for evaluation. For the image state, we utilize two metrics: **peak-signal-to-noise ratio (PSNR)** and **structure-similarity index measure (SSIM)** [25]. PSNR and SSIM are computed on the Y channel of the YCbCr representation for RGB images and the single channel for depth images. It is important to note that, based on prior knowledge of the AI2THOR environment, we normalize the reconstructed RGB images so that the brightest pixel has a value of 255, and the corresponding depth image is scaled by the same factor. In setting S2, the depth images are evaluated with their original pixel values. For the coordinate state, which represents a bounding box, we calculate the **intersection over union (IoU)** metric to measure accuracy. The accuracy of the action is evaluated by simply counting the number of accurate results. Lastly, we employ the **percentile error**, denoted as $\epsilon(x) = \frac{|x^{rec} - x|}{|x|}$, to evaluate the Q-value and target Q-value.

4.1 Quantitative Results

State: RGB and Depth Image. Table 1 presents the PSNR and SSIM values for the images. In the S1 setting, where both RGB and depth images are available, the mean PSNR of the RGB images is over 21dB, and the mean SSIM is over 0.7. These values indicate that the images are

Table 1: PSNR and SSIM of the RGB and depth images. The best results are underlined.

λ	State	Metric	bathroom	bedroom	kitchen	living room	average	best
$\lambda = 0.01$ (S1)	RGB	PSNR	14.10 ± 4.06	12.59 ± 3.22	15.28 ± 3.65	13.66 ± 3.88	13.91 ± 3.82	30.88
		SSIM	0.418 ± 0.162	0.422 ± 0.134	0.449 ± 0.149	0.415 ± 0.141	0.426 ± 0.147	0.886
	depth	PSNR	16.29 ± 5.78	14.91 ± 4.05	16.58 ± 4.52	14.47 ± 3.71	15.56 ± 4.64	36.04
		SSIM	0.404 ± 0.301	0.418 ± 0.283	0.443 ± 0.265	0.425 ± 0.242	0.422 ± 0.272	0.959
$\lambda = 0.1$ (S1)	RGB	PSNR	22.81 ± 5.99	19.73 ± 5.16	21.41 ± 5.69	20.11 ± 6.17	21.02 ± 5.86	<u>32.17</u>
		SSIM	0.761 ± 0.141	0.735 ± 0.146	0.724 ± 0.167	0.696 ± 0.170	0.729 ± 0.157	0.929
	depth	PSNR	24.89 ± 10.43	22.85 ± 7.42	23.26 ± 7.17	21.72 ± 7.05	23.18 ± 8.17	<u>38.09</u>
		SSIM	<u>0.809 ± 0.249</u>	<u>0.823 ± 0.161</u>	<u>0.803 ± 0.197</u>	<u>0.793 ± 0.162</u>	<u>0.807 ± 0.195</u>	<u>0.983</u>
adaptive λ (S1)	RGB	PSNR	<u>22.82 ± 3.67</u>	<u>20.02 ± 3.20</u>	<u>23.13 ± 3.92</u>	<u>21.11 ± 3.86</u>	<u>21.77 ± 3.87</u>	32.00
		SSIM	<u>0.764 ± 0.096</u>	<u>0.744 ± 0.092</u>	<u>0.757 ± 0.100</u>	<u>0.725 ± 0.089</u>	<u>0.747 ± 0.095</u>	0.937
	depth	PSNR	<u>26.54 ± 3.82</u>	<u>23.27 ± 4.19</u>	<u>25.20 ± 4.05</u>	<u>22.66 ± 3.64</u>	<u>24.42 ± 4.20</u>	34.52
		SSIM	<u>0.777 ± 0.109</u>	<u>0.762 ± 0.108</u>	<u>0.773 ± 0.107</u>	<u>0.738 ± 0.099</u>	<u>0.762 ± 0.106</u>	0.952
$\lambda = 0.1$ (S2)	depth	PSNR	29.78 ± 7.33	26.14 ± 7.67	26.45 ± 7.27	23.49 ± 7.29	26.46 ± 7.68	45.76
		SSIM	0.930 ± 0.111	0.899 ± 0.152	0.918 ± 0.092	<u>0.894 ± 0.129</u>	0.910 ± 0.123	0.994
adaptive λ (S2)	depth	PSNR	<u>31.61 ± 7.30</u>	<u>27.53 ± 7.41</u>	<u>29.82 ± 8.39</u>	<u>25.13 ± 7.02</u>	<u>28.52 ± 7.89</u>	48.24
		SSIM	<u>0.949 ± 0.049</u>	<u>0.916 ± 0.049</u>	<u>0.923 ± 0.078</u>	0.882 ± 0.137	<u>0.918 ± 0.095</u>	<u>0.998</u>

recognizable to humans, potentially leaking information about the layout of the environments and private elements to potential adversaries. The depth images exhibit higher PSNR and SSIM values than the RGB images, suggesting that the size of rooms and the distance of objects are at risk of privacy leakage. In the S2 setting, the adversary may find it more challenging to identify the room layout due to the lack of color information. However, the accuracy of the reconstructed depth images is significantly higher. As shown in Table 1, the PSNR and SSIM values increase by over 4dB for all room types, primarily due to the lower dimensionality of the input data. It is important to note that the bedroom and living room exhibit lower PSNR and SSIM values because these rooms in the AI2THOR simulator [20] contain more small objects, making the reconstruction of detailed patterns more challenging. For additional quantitative results, please refer to Appendix B.

Q-value and Target Q-value. Table 3 displays the percentile errors for the reconstructed Q-values and target Q-values. The results indicate that the percentile errors are significantly small, with an average mean error of less than 1.1% for both settings. It is worth noting that the bedrooms and living rooms exhibit larger errors in Q-value reconstruction. This suggests that when the image state contains more intricate details, the process of gradient inversion for the vector and scalar data becomes more challenging. This observation is further supported by the percentile errors observed in the S2 setting, which are approximately half of those in the S2 setting.

Action. The action identified from the gradient of a single sample is 100% correct in all 240 samples, which demonstrates the effectiveness of QGI in the decision-making task.

State: Coordinate. As shown in Table 2, the average IoU over of the 240 samples reaches over 0.9 for both S1 and S2 settings. The standard derivatives reach around 20% of the mean IoU, implying the reconstruction is not stable. To further study the variance of IoU, we demonstrate the histogram of IoU in Figure 3. For the S1 setting, 174 samples achieve IoU larger than 0.9999, while 217 samples achieve that in the S2 setting. The significant derivative arises due to the large error of failure cases, despite the occurrence of failure cases is limited. Coordinate reconstruction has higher accuracy than the images not only because of the lower dimension but also the fact that the coordinate is first processed by a linear layer other than a convolution layer.

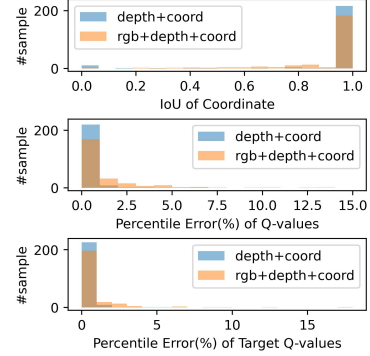


Figure 3: Histogram of coordinate IoU, percentile error of Q-values and target Q-values.

Table 2: IoU of coordinates.

Setting	bathroom	bedroom	kitchen	living room	average
RGB+depth+coord (S1)	0.933 ± 0.169	0.872 ± 0.229	0.949 ± 0.133	0.894 ± 0.212	0.912 ± 0.192
depth+coord (S2)	0.995 ± 0.028	0.970 ± 0.147	0.911 ± 0.264	0.887 ± 0.296	0.941 ± 0.217



Figure 4: Qualitative results. The left shows the results of depth+RGB images (S1). The right shows the results of depth images (S2).

4.2 Qualitative Results

The qualitative results shown in Figure 4 for the S1 setting are collected with λ 0.1, and the results for the S2 setting are collected under the adaptive method. In the left image of Figure 4, both the RGB images and depth images are reconstructed with recognizable patterns and magnitudes. The RGB images exhibit accurate color tones, although there may be some inaccurate colored noise in local areas. The depth images reconstructed in conjunction with the RGB images also display similar noisy patterns, but the overall brightness of continuous areas remains accurate. Consequently, the sizes of private rooms can be accessed by potential adversaries. In the S2 setting, as depicted in the right image of Figure 4, the successfully reconstructed images exhibit accuracy with clear edges and details. For additional qualitative results, please refer to Appendix B.

Table 3: Percentile error (%) of Q-values and target Q-values.

Setting	Metric	bathroom	bedroom	kitchen	living room	average
RGB+depth+coord (S1)	$\epsilon(\hat{Q})$	0.95 ± 1.70	1.35 ± 1.61	0.64 ± 1.10	1.19 ± 1.76	1.03 ± 1.59
	$\epsilon(Q)$	0.51 ± 0.97	0.89 ± 1.61	0.40 ± 1.03	0.40 ± 1.03	0.67 ± 1.47
depth+coord (S2)	$\epsilon(\hat{Q})$	0.11 ± 0.16	0.34 ± 0.62	0.45 ± 1.24	1.01 ± 2.54	0.48 ± 1.49
	$\epsilon(Q)$	0.11 ± 0.24	0.16 ± 0.30	0.25 ± 0.78	0.65 ± 0.24	0.29 ± 1.29

Table 4: Comparison of QGI and jointly optimizing (Joint) of vector and image states.

Method	PSNR/SSIM (RGB) \uparrow	PSNR/SSIM (depth) \uparrow	IoU \uparrow	$\epsilon(\hat{Q})(\%) \downarrow$	$\epsilon(Q)(\%) \downarrow$
Joint (S1)	$19.0 \pm 5.7/0.66 \pm 0.18$	$20.3 \pm 7.6/0.67 \pm 0.19$	0.057 ± 0.151	46.0 ± 11.8	27.2 ± 37.6
QGI (S1)	$21.8 \pm 3.9/0.74 \pm 0.10$	$24.4 \pm 4.2/0.76 \pm 0.11$	0.912 ± 0.192	1.03 ± 1.59	0.67 ± 1.47

4.3 Ablation Study

We evaluate the effect of the proposed QGI by comparing it with joint optimization. The joint optimization is applied to the state reconstruction step, jointly optimizing the vector and image reconstruction. As shown in Table 4, the joint optimization of the image state (RGB+depth) and vector state (goal coordinate) shows performance drops in terms of all metrics. The mean IoU is below 0.1, while QGI achieves over 0.9. The Q-value reconstruction also shows significant errors in joint optimization, and the mean $\epsilon(\hat{Q})$ increases over 40 times compared to QGI.

We then investigate the adaptive weight in L_{img} by comparing QGI with constants $\lambda = 0.1, 0.01$. In the S1 setting, the adaptive weighted method shows a slight improvement in the PSNR and SSIM in Table 1. However, we find the visual quality of the $\lambda = 0.1$ is more stable than the adaptive λ , despite the larger standard derivative of PSNR and SSIM. For depth images in both settings, the

adaptive λ shows a consistent advantage over the constant λ in Table 1 and the visual quality is stable as shown in Figure 4, especially in the S2 setting.

5 Related Work

Privacy attack in Deep Learning. Private training data is at risk of attacks, including membership inference, model inversion, and gradient inversion [26]. Membership inference assumes the adversary has access to certain data and attempts to verify whether the data is used in the training procedure [27, 28], while in robotic tasks, the private environments tend to stay inaccessible to adversaries, for example, bedrooms of private property. In contrast, model inversion and gradient inversion assume the private data is inaccessible and the adversary attempts to reconstruct the data, which are of higher significance for robotic tasks. While model inversion reveals the training data from the trained model [29, 30, 19, 31], gradient inversion tackles the reconstructing from the gradients shared in federated, collaborative, decentralized, or distributed learning [10, 11, 16, 14, 32, 12].

Gradient inversion. Previous works in gradient inversion mainly focused on image classification tasks. Zhu et al. [10] proposed an end-to-end optimization method to recover both images and labels for the classification task from both single sample gradients and batched gradients. Zhao et al. [13] proposed an efficient method to identify the one-hot label from a single sample’s gradient. Geiping et al. [11] extended gradient inversion to high-resolution images by minimizing a prior loss proven effective in image denoising [24] and model inversion [30] and a magnitude-agnostic cost function. Yin et al. [16] increased the accuracy under large batch sizes by leveraging more image prior loss functions and penalizing distances of results from multiple trials. While most works studied gradient inversion on CNN or MLP, GradViT [12] attacked gradients of Vision Transformer by designing prior terms aiming at the architecture. Wang et al. [15] and Jeon et al. [14] enhanced the gradient inversion by introducing a generative network. Based on [10], Deng et al. [33] reconstructed training data of Transformer-based language models. Despite the achievement, to the best of our knowledge, gradient inversion is unexplored in the realm of both robotic tasks and multi-modal data.

Privacy in Reinforcement Learning. Privacy has been studied in existing Reinforcement Learning literature for a long time. However, most works dedicated to privacy-preserving [3, 34, 4, 35, 36] other than revealing the risk of privacy leakage. The most pertinent work to this paper in Reinforcement Learning is the [17]. They recovered the training environment from the trained policies, demonstrating the privacy risk of releasing trained models. In contrast to model inversion algorithms oriented towards supervised learning, typically utilizing gradient-descent-based optimization methods, they leveraged the prior knowledge of the environment and used the genetic algorithm to search for the environment configuration. While they studied the sensitive information contained in trained models, the risk associated with the training procedure remains ambiguous. In this work, we investigate the possibility of revealing private state, action, and Q-values from gradients, where the data can change through the training procedure and the number of data samples is unlimited.

6 Conclusion and Limitation

This paper introduces a novel method called QGI to address the issue of privacy leakage in DQN, which is a critical concern but has not received significant attention in the existing literature. Given the challenge of adapting existing gradient inversion algorithms to handle multi-modal inputs in RL, we develop a comprehensive pipeline that iteratively recovers the inputs. Through experimental results in active perception tasks, we demonstrate that QGI successfully recovers the image state, vector state, action, and Q-value from the gradient of the model. Ablation studies further validate that our proposed design outperforms baseline models.

One limitation of this work is that the batch size of the input data is constrained to a small number in order to maintain the high quality of the recovered data. As pioneers in this area, we recognize the significance of addressing the privacy problem in decision-making to establish a trustworthy embodied AI system. Therefore, we leave the exploration of larger batch sizes and extensions to other RL-based decision-making algorithms for future research.

References

- [1] L. Ouyang, J. Wu, X. Jiang, D. Almeida, C. Wainwright, P. Mishkin, C. Zhang, S. Agarwal, K. Slama, A. Ray, et al. Training language models to follow instructions with human feedback. *Advances in Neural Information Processing Systems*, 35:27730–27744, 2022.
- [2] A. Ramesh, P. Dhariwal, A. Nichol, C. Chu, and M. Chen. Hierarchical text-conditional image generation with clip latents. *arXiv preprint arXiv:2204.06125*, 2022.
- [3] J. Sakuma, S. Kobayashi, and R. N. Wright. Privacy-preserving reinforcement learning. In *Proceedings of the 25th international conference on Machine learning*, pages 864–871, 2008.
- [4] B. Wang and N. Hegde. Privacy-preserving q-learning with functional noise in continuous spaces. *Advances in Neural Information Processing Systems*, 32, 2019.
- [5] C. Zhang, Y. Xie, H. Bai, B. Yu, W. Li, and Y. Gao. A survey on federated learning. *Knowledge-Based Systems*, 216:106775, 2021.
- [6] B. McMahan, E. Moore, D. Ramage, S. Hampson, and B. A. y Arcas. Communication-efficient learning of deep networks from decentralized data. In *Artificial intelligence and statistics*, pages 1273–1282. PMLR, 2017.
- [7] J. Konečný, B. McMahan, and D. Ramage. Federated optimization: Distributed optimization beyond the datacenter. *arXiv preprint arXiv:1511.03575*, 2015.
- [8] J. Konečný, H. B. McMahan, D. Ramage, and P. Richtárik. Federated optimization: Distributed machine learning for on-device intelligence. *arXiv preprint arXiv:1610.02527*, 2016.
- [9] S. Reddi, Z. Charles, M. Zaheer, Z. Garrett, K. Rush, J. Konečný, S. Kumar, and H. B. McMahan. Adaptive federated optimization. *arXiv preprint arXiv:2003.00295*, 2020.
- [10] L. Zhu, Z. Liu, and S. Han. Deep leakage from gradients. *Advances in neural information processing systems*, 32, 2019.
- [11] J. Geiping, H. Bauermeister, H. Dröge, and M. Moeller. Inverting gradients-how easy is it to break privacy in federated learning? *Advances in Neural Information Processing Systems*, 33: 16937–16947, 2020.
- [12] A. Hatamizadeh, H. Yin, H. R. Roth, W. Li, J. Kautz, D. Xu, and P. Molchanov. Gradvit: Gradient inversion of vision transformers. In *Proceedings of the IEEE/CVF Conference on Computer Vision and Pattern Recognition*, pages 10021–10030, 2022.
- [13] B. Zhao, K. R. Mopuri, and H. Bilen. idlg: Improved deep leakage from gradients. *arXiv preprint arXiv:2001.02610*, 2020.
- [14] J. Jeon, K. Lee, S. Oh, J. Ok, et al. Gradient inversion with generative image prior. *Advances in neural information processing systems*, 34:29898–29908, 2021.
- [15] Z. Wang, M. Song, Z. Zhang, Y. Song, Q. Wang, and H. Qi. Beyond inferring class representatives: User-level privacy leakage from federated learning. In *IEEE INFOCOM 2019-IEEE conference on computer communications*, pages 2512–2520. IEEE, 2019.
- [16] H. Yin, A. Mallya, A. Vahdat, J. M. Alvarez, J. Kautz, and P. Molchanov. See through gradients: Image batch recovery via gradinversion. In *Proceedings of the IEEE/CVF Conference on Computer Vision and Pattern Recognition*, pages 16337–16346, 2021.
- [17] X. Pan, W. Wang, X. Zhang, B. Li, J. Yi, and D. Song. How you act tells a lot: Privacy-leaking attack on deep reinforcement learning. In *AAMAS*, pages 368–376, 2019.

- [18] V. Mnih, K. Kavukcuoglu, D. Silver, A. A. Rusu, J. Veness, M. G. Bellemare, A. Graves, M. Riedmiller, A. K. Fidjeland, G. Ostrovski, et al. Human-level control through deep reinforcement learning. *nature*, 518(7540):529–533, 2015.
- [19] B. Hitaj, G. Ateniese, and F. Perez-Cruz. Deep models under the gan: information leakage from collaborative deep learning. In *Proceedings of the 2017 ACM SIGSAC conference on computer and communications security*, pages 603–618, 2017.
- [20] E. Kolve, R. Mottaghi, W. Han, E. VanderBilt, L. Weihs, A. Herrasti, M. Deitke, K. Ehsani, D. Gordon, Y. Zhu, et al. Ai2-thor: An interactive 3d environment for visual ai. *arXiv preprint arXiv:1712.05474*, 2017.
- [21] W. Ding, N. Majcherczyk, M. Deshpande, X. Qi, D. Zhao, R. Madhivanan, and A. Sen. Learning to view: Decision transformers for active object detection. *arXiv preprint arXiv:2301.09544*, 2023.
- [22] K. Kotar and R. Mottaghi. Interactron: Embodied adaptive object detection. In *Proceedings of the IEEE/CVF Conference on Computer Vision and Pattern Recognition*, pages 14860–14869, 2022.
- [23] P. Ammirato, P. Poirson, E. Park, J. Koščeká, and A. C. Berg. A dataset for developing and benchmarking active vision. In *2017 IEEE International Conference on Robotics and Automation (ICRA)*, pages 1378–1385. IEEE, 2017.
- [24] L. I. Rudin, S. Osher, and E. Fatemi. Nonlinear total variation based noise removal algorithms. *Physica D: nonlinear phenomena*, 60(1-4):259–268, 1992.
- [25] Z. Wang, A. C. Bovik, H. R. Sheikh, and E. P. Simoncelli. Image quality assessment: from error visibility to structural similarity. *IEEE transactions on image processing*, 13(4):600–612, 2004.
- [26] M. Rigaki and S. Garcia. A survey of privacy attacks in machine learning. *arXiv preprint arXiv:2007.07646*, 2020.
- [27] R. Shokri, M. Stronati, C. Song, and V. Shmatikov. Membership inference attacks against machine learning models. In *2017 IEEE symposium on security and privacy (SP)*, pages 3–18. IEEE, 2017.
- [28] N. Carlini, F. Tramer, E. Wallace, M. Jagielski, A. Herbert-Voss, K. Lee, A. Roberts, T. B. Brown, D. Song, U. Erlingsson, et al. Extracting training data from large language models. In *USENIX Security Symposium*, volume 6, 2021.
- [29] S. An, G. Tao, Q. Xu, Y. Liu, G. Shen, Y. Yao, J. Xu, and X. Zhang. Mirror: Model inversion for deep learning network with high fidelity. In *Proceedings of the 29th Network and Distributed System Security Symposium*, 2022.
- [30] A. Mordvintsev, C. Olah, and M. Tyka. Inceptionism: Going deeper into neural networks. 2015.
- [31] H. Yin, P. Molchanov, J. M. Alvarez, Z. Li, A. Mallya, D. Hoiem, N. K. Jha, and J. Kautz. Dreaming to distill: Data-free knowledge transfer via deepinversion. In *Proceedings of the IEEE/CVF Conference on Computer Vision and Pattern Recognition*, pages 8715–8724, 2020.
- [32] X. Jin, P.-Y. Chen, C.-Y. Hsu, C.-M. Yu, and T. Chen. Cafe: Catastrophic data leakage in vertical federated learning. *Advances in Neural Information Processing Systems*, 34:994–1006, 2021.
- [33] J. Deng, Y. Wang, J. Li, C. Shang, H. Liu, S. Rajasekaran, and C. Ding. Tag: Gradient attack on transformer-based language models. *arXiv preprint arXiv:2103.06819*, 2021.

- [34] G. Vietri, B. Balle, A. Krishnamurthy, and S. Wu. Private reinforcement learning with pac and regret guarantees. In *International Conference on Machine Learning*, pages 9754–9764. PMLR, 2020.
- [35] E. Garcelon, V. Perchet, C. Pike-Burke, and M. Pirotta. Local differential privacy for regret minimization in reinforcement learning. *Advances in Neural Information Processing Systems*, 34:10561–10573, 2021.
- [36] M. Taherisadr, S. A. Stavroulakis, and S. Elmalaki. adaparl: Adaptive privacy-aware reinforcement learning for sequential-decision making human-in-the-loop systems. *arXiv preprint arXiv:2303.04257*, 2023.

A DQN Model Structure

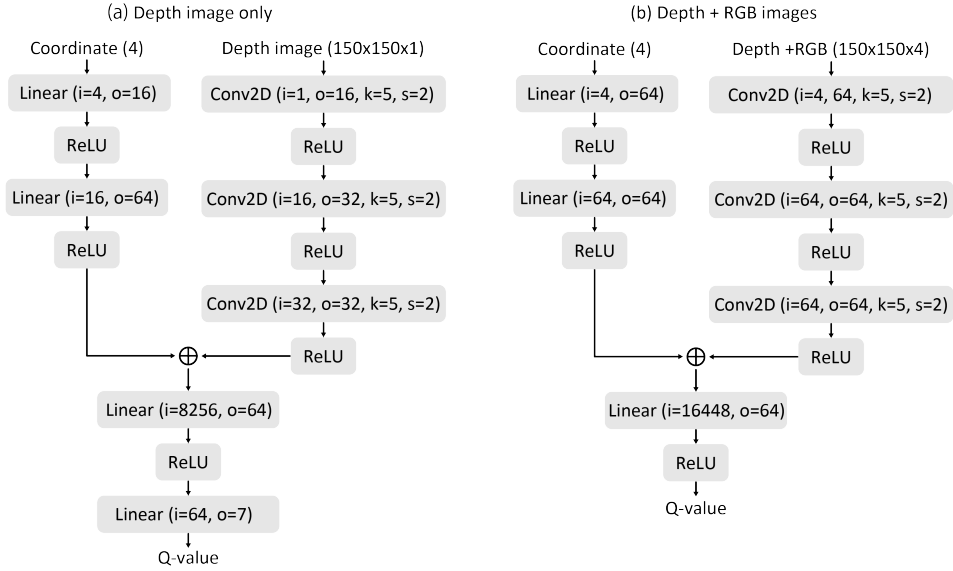


Figure 5: The model structure of the depth-only network and the depth+RGB network.

B More Experimental Results

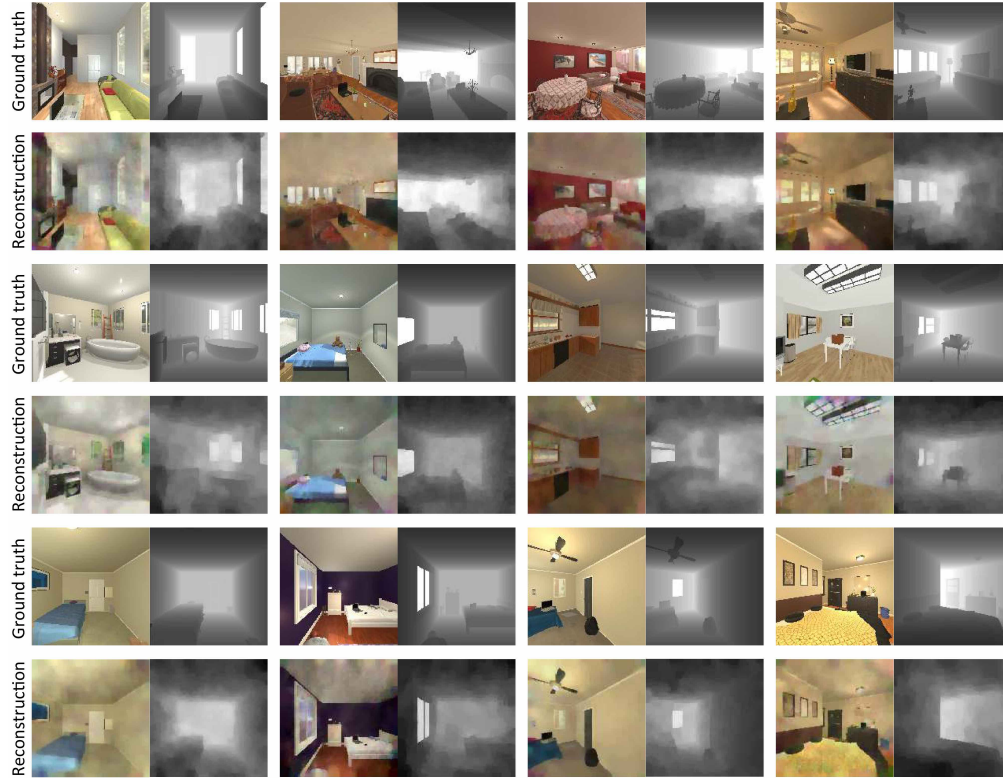


Figure 6: More qualitative results of the depth+RGB image (S1)setting.

We demonstrate more qualitative results of the depth+RGB image setting and the depth-only image setting in Figure 6 and Figure 7, respectively.

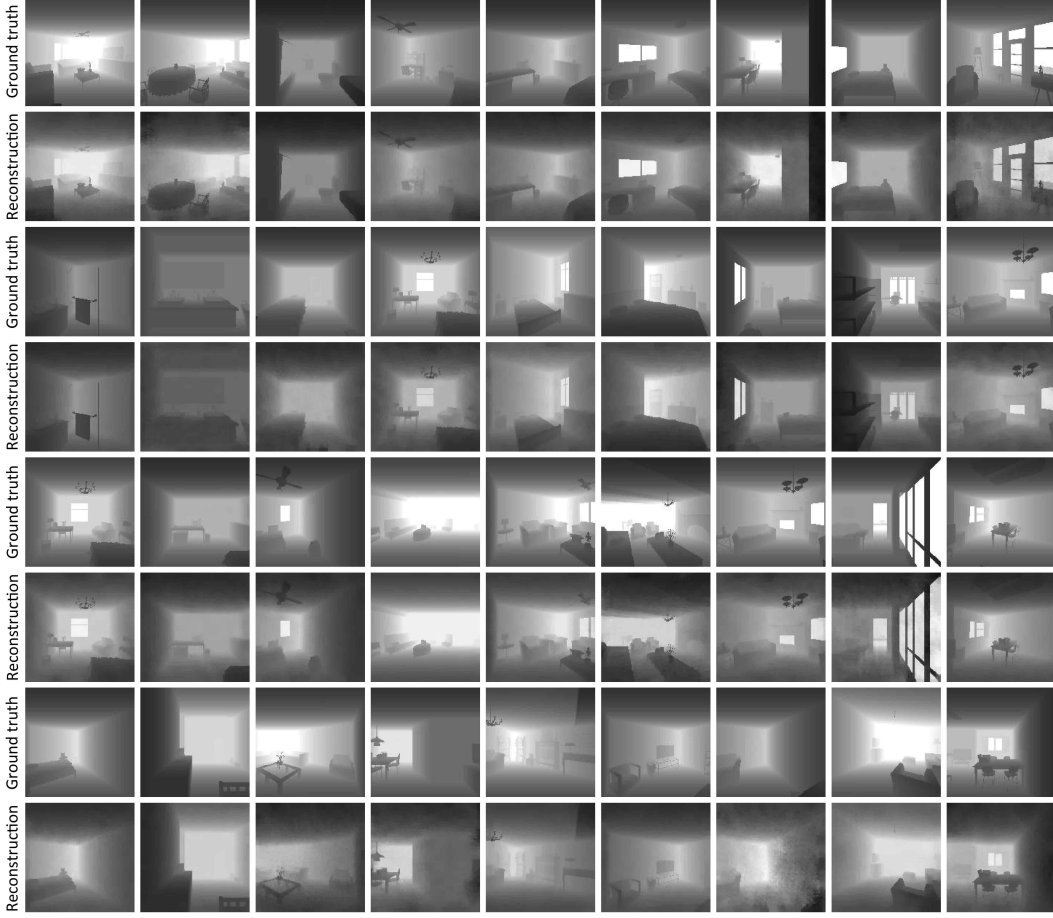


Figure 7: More qualitative results of the depth-only image (S2) setting.

We also investigate the possibility of gradient inversion on a **trained** network. Figure 9 shows depth image reconstruction from gradients of a trained DQN, which demonstrates some of the most recognizable results. The edges and details are reconstructed with high fidelity and depth estimations are comparable with the ground truth.

The gradient matching loss values are shown in Table 5. Specifically, we record the smallest gradient matching loss for each sample during the iteration and calculate the mean and standard derivative. As shown in the first and second rows, the gradient matching loss values of the vector state reconstruction are much smaller than the image reconstruction stage, consistent with the statement that gradient inversion of the convolution layer is more challenging than the linear layer. Note that the vector reconstruction stage results of the S1 are smaller than the results in the S2 because the network used in thing S1 has more parameters than the network used in the S2 setting, providing more information about the training data. For the image reconstruction stage, the loss values of S1 are larger than the S2, indicating the reconstruction of both RGB and depth images is more challenging than reconstructing only the depth image, due to the larger dimension of data. As shown in Figure 8, 235(S1) and 228(S2) out of the 240 samples have the smallest gradient matching loss reaching 0 in the vector state reconstruction stage, while in the image state reconstruction stage, no gradient matching loss can converge to 0. Although joint optimization achieves a smaller mean result than the proposed QGI, as shown in Table 5, the histogram shows that QGI tends to generate reconstructions

Table 5: Gradient Matching Loss for vector state reconstruction and image state reconstruction.

method	vector state reconstruction	image state reconstruction
QGI (S2)	$1.206 \times 10^{-5} \pm 1.139 \times 10^{-4}$	$7.364 \times 10^{-4} \pm 1.462 \times 10^{-3}$
QGI (S1)	$7.778 \times 10^{-7} \pm 1.058 \times 10^{-5}$	$2.518 \times 10^{-3} \pm 2.129$
joint (S1)	$2.094 \times 10^{-3} \pm 1.385 \times 10^{-3}$	

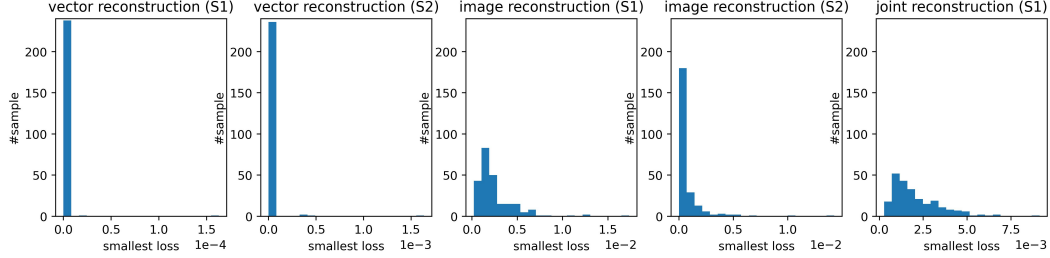


Figure 8: Histogram of smallest gradient matching loss values for state reconstruction in S1 and S2 settings.

with small gradient matching losses, while joint optimization of vector and joint results in more large results.



Figure 9: Qualitative results of depth images (S2) on trained DQN.

C Experiment Settings

The optimization is conducted by AdamW optimizer with betas= (0.9, 0.999). The learning rate is initialized to 0.1 and decays during the iteration. For the vector state reconstruction, the learning rate decays by 10 times at iteration 8×10^3 and 1.6×10^4 . For the image state reconstruction, the learning rate decays by 10 times at iteration 4×10^3 , 1×10^4 , and 1.6×10^4 . We find the update of the state is unstable and thus, we only preserve the sign of the state gradient, for example, $\text{sign}(\frac{\partial L}{\partial s_c})$ to use as final gradient passing to the optimizer. We also clip the reconstructed image state s_i^{rec} and s_d^{rec} in every iteration to force the search space lying inside $[0, 1]^{150 \times 150}$. The final vector state reconstruction is selected by locating the smallest gradient matching loss. The final image state is selected by locating the smallest gradient matching loss and the smallest TV loss, resulting in 2 image reconstructions for each image state. To obtain the quantitative result, the

same evaluation is conducted for the 2 images, and the better one is used for the mean, standard derivative, and maximum value calculation. Note that the 2 reconstructed images are considerably similar. Moreover, the adversary can retrieve both images to steal private information and our goal is to demonstrate the potential risk.

All of our experiments are conducted on a machine with $2\times$ AMD EPYC 7542 32-Core CPU, an NVIDIA RTX A6000 GPU (48GB memory), and 256GB memory.

D More Explanation on Method

Gradient inversion aims to reconstruct the training data by optimizing the reconstructed data to mimic the true gradient. Given the Q-network, the gradient is

$$g = \frac{\partial J(\hat{Q}, Q)}{\partial \hat{Q}} \frac{\partial \hat{Q}}{\partial w} = 2(\hat{Q} - Q) \frac{\partial \hat{Q}}{\partial w}. \quad (8)$$

The gradient contains 2 components, namely $2(\hat{Q} - Q)$ and $\frac{\partial \hat{Q}}{\partial w}$. A sufficiently accurate estimation of the first term can accelerate the optimization of the gradient matching loss, specifically, mimicking the second term by reconstructing the training data. We find in experiments that an accurate $2(\hat{Q} - Q)$ reconstruction is more beneficial than an accurate supervision signal Q reconstruction. Moreover, observing that the magnitude of $\hat{Q} - Q$ has no influence on the gradient matching loss L , we propose to first reconstruct the sign $\vec{n} = \hat{Q} - Q$, and use the reconstructed sign in the reconstruction of the vector and the image state. The usage of \vec{n} during the state reconstruction is conducted by defining a constant \tilde{Q} as the temporary reconstruction of the target Q-value, which is sufficiently large and thus the reconstructed error $\hat{Q}^{rec} - \tilde{Q}$ has the sign \vec{n} .